

Backsplash galaxies and their impact on galaxy evolution: a three-stage, four-type perspective

Andrés N. Ruiz,^{1,2*} Héctor J. Martínez,^{1,2} Valeria Coenda,^{1,2} Hernán Muriel,^{1,2} Sofía A. Cora,^{3,4} Martín de los Ríos,^{5,6} and Cristian A. Vega-Martínez^{7,8}

¹*Instituto de Astronomía Teórica y Experimental (CONICET-UNC), Laprida 854, X5000BGR, Córdoba, Argentina*

²*Observatorio Astronómico, Universidad Nacional de Córdoba, Laprida 854, X5000BGR, Córdoba, Argentina*

³*Instituto de Astrofísica de La Plata (CONICET-UNLP), Observatorio Astronómico, Paseo del Bosque S/N, B1900FWA, La Plata, Argentina*

⁴*Facultad de Ciencias Astronómicas y Geofísicas, Universidad Nacional de La Plata, Observatorio Astronómico, Paseo del Bosque S/N, B1900FWA, La Plata, Argentina*

⁵*Departamento de Física Teórica, Universidad Autónoma de Madrid, 28049 Madrid, Spain*

⁶*Instituto de Física Teórica, IFT-UAM/CSIC, C/ Nicolás Cabrera 13-15, Universidad Autónoma de Madrid, Cantoblanco, Madrid 28049, Spain*

⁷*Instituto Multidisciplinario de Investigación y Postgrado, Universidad de La Serena, Raúl Bitrán 1305, La Serena, Chile*

⁸*Departamento de Astronomía, Universidad de La Serena, Av. Juan Cisternas 1200 Norte, La Serena, Chile*

26 July 2023

ABSTRACT

We study the population of backsplash galaxies at $z = 0$ in the outskirts of massive, isolated clusters of galaxies taken from the MDPL2-SAG semi-analytic catalogue. We consider four types of backsplash galaxies according to whether they are forming stars or passive at three stages in their lifetimes: before entering the cluster, during their first incursion through the cluster, and after they exit the cluster. We analyse several geometric, dynamic, and astrophysical aspects of the four types at the three stages. Galaxies that form stars at all stages account for the majority of the backsplash population (58%) and have stellar masses typically below $M_{\star} \sim 3 \times 10^{10} h^{-1} M_{\odot}$ that avoid the innermost cluster’s regions and are only mildly affected by it. In a similar mass range, galaxies that become passive after exiting the cluster (26%) follow orbits characterised by small pericentric distance and a strong deflection by the cluster potential well while suffering a strong loss of both dark matter and gas content. Only a small fraction of our sample (4%) become passive while orbiting inside the cluster. These galaxies have experienced heavy pre-processing and the cluster’s tidal stripping and ram pressure provide the final blow to their star formation. Finally, galaxies that are passive before entering the cluster for the first time (12%) are typically massive and are not affected significantly by the cluster. Using the bulge/total mass ratio as a proxy for morphology, we find that a single incursion through a cluster do not result in significant morphological changes in all four types.

Key words: galaxies: clusters: general – galaxies: haloes – galaxies: kinematics and dynamics – galaxies: evolution – methods: numerical – methods: statistical

1 INTRODUCTION

For several decades, the study of galaxy clusters and their impact on the galaxy evolution has remained as a captivating research subject. The process of galaxy evolution within clusters involves a myriad of physical mechanisms that operate across varying spatial and temporal scales. Both internal and environmental factors exert significant influence on the characteristics of galaxies, giving rise to a wide range of possible transformations and adaptations. Supernovae (e.g. Stringer et al. 2012, Bower et al. 2012, Christensen et al. 2016), active nuclei (e.g. Nandra et al. 2007, Hasinger 2008, Silverman et al. 2008, Cimatti et al. 2013), and

stellar feedback (e.g. Dalla Vecchia & Schaye 2008, Hopkins et al. 2012) are among the internal mechanisms that impact galaxies. On the other hand, properties of galaxies, such as star formation (e.g. Hashimoto et al. 1998; Mateus & Sodré 2004; Blanton & Moustakas 2009; Welikala et al. 2008; Schaefer et al. 2017; Coenda et al. 2019), morphology (e.g. Dressler 1980; Whitmore, Gilmore & Jones 1993; Domínguez, Muriel & Lambas 2001; Weinmann et al. 2006; Bamford et al. 2009; Paulino-Afonso et al. 2019), luminosity (e.g. Adami, Biviano & Mazure 1998; Coenda et al. 2006), color (e.g. Blanton et al. 2005; Martínez & Muriel 2006; Martínez, Coenda & Muriel 2008), age (e.g. Thomas et al. 2005, Cooper et al. 2010, Zheng et al. 2017), are significantly influenced by their environment.

* andres.ruiz@unc.edu.ar

Several mechanisms impact galaxies in clusters, some of

which cause gas depletion and the halt of star formation. Galaxies that move at high velocities through the intra-cluster medium (ICM) experience ram pressure stripping (e.g. Gunn & Gott 1972; Abadi, Moore & Bower 1999; Book & Benson 2010; Steinhauser, Schindler & Springel 2016), which removes a significant portion of their cold gas and reduces their star formation rate (SFR). Moreover, a galaxy's trip through the ICM can result in the removal of its warm gas, a phenomenon known as starvation (Larson et al. 1980; McCarthy et al. 2008; Bekki 2009; Bahé et al. 2013; Vijayaraghavan & Ricker 2015). Starvation inhibits future star formation by cutting off the supply of gas that cools from the galaxy's halo. Tidal stripping from the cluster potential is another mechanism that eliminates the gas supply (Zwicky 1951; Gnedin 2003a; Villalobos, De Lucia & Murante 2014). In contrast, in intermediate-density areas such as cluster outskirts and groups, harassment is a more effective galaxy-galaxy interaction mechanism (e.g. Moore et al. 1996; Moore et al. 1998, Gnedin 2003b). It causes both gas depletion and morphological transformations. Tidal stripping from galaxy-galaxy encounters can truncate galaxies, mainly disks, and result in spheroid-dominated galaxies (e.g. Smith et al. 2015). Morphological evolution primarily depends on mergers (e.g. Toomre 1977; Barnes 1992; Di Matteo et al. 2007; Martin et al. 2018), with gas-rich minor mergers producing massive disks (Jackson et al. 2022), and with major mergers resulting in spheroidal systems (Navarro & White 1994).

Galaxies may encounter various environmental conditions and be subjected to one or more of the mechanisms discussed earlier at different stages of their life cycle. As galaxies fall towards clusters, they can experience different physical processes depending on whether they are part of a group (e.g. McGee et al. 2009; De Lucia et al. 2012; Wetzel et al. 2013; Hou, Parker & Harris 2014), falling from the field (e.g. Berrier et al. 2009), or through filament streams (e.g. Colberg et al. 1999; Ebeling et al. 2004; Martínez et al. 2016; Rost et al. 2020; Kuchner et al. 2022). Before entering the cluster, galaxies can undergo several physical transformations due to these processes, which are collectively called pre-processing (e.g. Mihos 2004; Fujita 2004).

After being incorporated into a cluster, galaxies have two possible outcomes: they can either remain bound to the cluster's gravitational field or their trajectory can carry them away from the cluster, spanning distances of up to several R_{200} , the radius enclosing 200 times the mean density of the Universe (e.g. Mamon et al. 2004; Gill et al. 2005; Rines & Diaferio 2006; Aguerri & Sánchez-Janssen 2010; Muriel & Coenda 2014; Casey et al. 2023). Eventually, these galaxies will turn around and fall back into the cluster during a subsequent infall. This unique population of galaxies is known as backsplash galaxies (Balogh et al. 2000). These particular galaxies can be used as laboratories to explore the impact of the cluster environment in galaxy properties, and to disentangle which stage is more important in their lifetimes. However, after these galaxies left the cluster, they may show characteristics of "post-processing" that are difficult to distinguish from "pre-processing" signatures. In addition, observational studies have demonstrated that environmental effects may extend beyond the halo boundary to impact both baryonic components (e.g. Wetzel et al. 2012; Lu et al. 2012) and dark matter haloes (e.g. Behroozi et al. 2014).

In the last years there have been many works about backsplash galaxies from a theoretical perspective. Benavides et al. (2021), using the ILLUSTRISTNG hydrodynamical simulations (Pillepich et al. 2018; Nelson et al. 2018; Naiman et al. 2018; Marinacci et al. 2018; Springel et al. 2018), have found that backsplash galaxies that were in the past satellite of another group or cluster, can be the origin

of quenched ultra-diffuse galaxies. Kuchner et al. (2022) explores the concept of backsplash galaxies that are falling into clusters along filaments. For the authors, these are galaxies outside the R_{200} that remain gravitationally bound to the cluster, and they may have made several orbits around the potential center. The study reveals that between 30 to 60 per cent of filament galaxies are classified as backsplash galaxies. Interestingly, backsplash galaxies return to the cluster after deviating significantly from their initial trajectory upon entry, particularly in more relaxed clusters. They do not exhibit a preferred location with respect to filaments and are unable to collapse and form filaments themselves. Several studies of backsplash galaxies around clusters have been carried out using THE THREEHUNDRED project (Cui et al. 2018), a suite of hydrodynamical resimulations of galaxy clusters. Haggard et al. (2020) found that the fraction of backsplash galaxies inhabiting a shell between R_{200} and $2R_{200}$ vary from 21 to 85 per cent, with a mean value of 58 per cent, and that this fraction is dependent of the dynamical state of the cluster. Knebe et al. (2020) perform a detailed study of the shape and alignment of galaxies around clusters, finding that backsplash galaxies have a larger radial alignment and more spherical shapes than the infalling population of galaxies. Hough et al. (2023) discovered that approximately 65 per cent of quenched galaxies situated near clusters are backsplash galaxies. This suggests that a combination of ram pressure stripping during the pre-processing stage and within the cluster is required to suppress star formation. Recently, Borrow et al. (2023), use ILLUSTRISTNG simulations to study backsplash galaxies around 1302 isolated galaxy clusters with mass $10^{13.0} < M_{200}/M_{\odot} < 10^{15.5}$. Their studies show that backsplash galaxies exhibit distinct characteristics compared to field galaxies, such as low gas fractions, high mass-to-light ratios, large stellar sizes, and low black hole occupation fractions.

The aim of this study is to investigate the existence and consequences of pre-processing in backsplash galaxies that have yet to cross the virial radius, as well as the effects of clusters on their subsequent evolution, once they are situated in the outskirts. Specifically, this research delves into the life cycle of these galaxies starting from 2 Gyr prior to their initial crossing of the virial radius. The present paper is organised as follows. In Sec. 2 we describe the simulated galaxy catalogue and define the types and stages considered. Dynamical and astrophysical properties of BS galaxies are analysed in Sec. 3 and 4, respectively. Finally, in Sec. 5 we present the main remarks of our work.

2 DATA

To construct our sample of simulated galaxy clusters, we have combined dark matter-only simulations of regions that contain cluster-like haloes at $z = 0$ taken from the MDPL2 cosmological simulation, along with the semi-analytic model of galaxy formation SAG. In this regard, we will first provide a brief overview of the dark matter simulation and the semi-analytic model, followed by a description of the selection criteria employed to construct the galaxy sample in and around clusters.

2.1 The MDPL2 cosmological simulation

The MDPL2 cosmological simulation is one of several simulations within the MULTIDARK suite (Riebe et al. 2013; Klypin et al. 2016). This simulation contains 3840^3 dark matter particles in a comoving cubic box measuring $1h^{-1}$ Gpc in length on each side. Each particle has a mass of $m_p = 1.51 \times 10^9 h^{-1} M_{\odot}$. The simulation assumes

a flat Λ CDM cosmology with $\Omega_m = 0.307$, $h = 0.678$, $n = 0.96$, and $\sigma_8 = 0.823$, which is consistent with measurements made by Planck Collaboration et al. (2014, 2016). Using GADGET-2 (Springel 2005), the simulation tracks the dynamical evolution of dark matter particles from an initial redshift $z = 120$. Over the course of the simulation, 126 snapshots were recorded between redshifts $z = 17$ and $z = 0$.

Dark matter haloes and subhaloes were identified using the ROCKSTAR phase-space halo finder (Behroozi et al. 2013a), and merger trees were constructed using CONSISTENT TREES (Behroozi et al. 2013b). The halo/subhalo catalogues and merger trees used in this study are publicly accessible through the COSMOSIM¹ and SKIES&UNIVERSES² databases, and form the foundation of the semi-analytic model for generating the galaxy population.

2.2 The SAG model

The semi-analytic model of galaxy formation and evolution SAG (acronym for Semi-Analytic Galaxies) has its roots in the model presented by Springel et al. (2001); the most recent version is described in Cora et al. (2018). It simulates the formation and growth of galaxies within each detected dark matter halo, tracking the evolution of galaxy properties through the merger trees of haloes and subhaloes. The model can be used to study a wide range of galaxy properties, including their luminosity functions, mass functions, star formation histories, and morphologies. The SAG model incorporates physical processes such as gas cooling, star formation and chemical enrichment. Star formation proceeds in both quiescent and bursty modes; the former takes place in gaseous discs, and the latter is triggered by disc instabilities and mergers contributing to the formation of a stellar bulge and the growth of a central supermassive black hole. Feedback processes from both supernovae and active galactic nuclei are also included.

One of the key strengths of the SAG model is its ability to incorporate environmental effects, such as ram pressure stripping (RPS) and tidal stripping, on galaxy properties. These effects occur predominantly within groups and clusters, which is particularly relevant to the current investigation. Upon becoming satellites, galaxies retain a hot gas halo that is gradually removed by various processes, with RPS being the primary contributor. As a result, the hot gas halo of a satellite galaxy serves as a protective barrier against the effects of the ram pressure exerted by the intragroup/intracluster medium on the cold gas located within the galaxy's disc. This protective function persists provided that the ratio between the hot gas halo and the galaxy's baryonic mass is greater than 0.1. Nonetheless, if this ratio drops below the aforementioned threshold, the hot gas halo is considered exhausted, which enables ram pressure to strip the cold gas disc. The application of RPS relies on a novel analytical fitting profile, which simulates the force of ram pressure acting upon satellite galaxies in distinct environments (characterized by the dark matter halo mass), at different halocentric distances and redshifts (Vega-Martínez et al. 2022).

The SAG model accounts for orphan galaxies by monitoring satellites left over from haloes that the underlying simulation can no longer resolve. It uses the information provided by an orbital evolution model that encompasses both dynamical friction and mass-loss by tidal stripping (Delfino et al. 2022). Although the calibration of

the model, that is, the fine adjustment of the free parameters associated with certain implemented physical processes, takes orphan satellites into account, they are not included in the sample analyzed in this study.

The calibration is accomplished by utilizing the Particle Swarm Optimization technique (Ruiz et al. 2015), which yields a set of best-fitting values for the free parameters by comparing the model results against a given set of observables. The galaxy properties considered for calibration include the stellar mass functions at redshifts $z = 0$ and $z = 2$, the distribution function of star formation rates at $z = 0.15$, the percentage of cold gas mass as a function of stellar mass at $z = 0$, and the correlation between bulge mass and the mass of the central supermassive black hole at $z = 0$. Table 1 in Cora et al. (2018) displays the values of the free parameters defining the model version utilized in this study, with the exception of the parameter responsible for regulating the redshift dependence of the reheated and ejected cold gas by supernova feedback (parameter β ; see their Eqs. 10 and 12). This parameter has been reduced to enhance the agreement between the simulated and observed values of the evolution of the star formation rate density and the fraction of quenched galaxies as a function of stellar and halo mass, which are predictions of the model (see, respectively, their Figs. 6 and 11). During the calibration process, the fit to the stellar mass function at $z = 2$ results in $\beta = 1.99$, which favours larger supernova feedback efficiency at higher redshifts and, consequently, a reduction of the star formation activity at those redshifts; this activity is shifted to later epochs and $z = 0$ galaxies have less time to be quenched. A better agreement between the aforementioned model predictions and observational data is obtained by fixing $\beta = 1.3$ while keeping the rest of the parameter values from the calibration process, at the expense of predicting a higher number density of low-mass galaxies in the stellar mass function at $z = 2$. This smaller value of β is provided by the FIRE hydrodynamical simulations of Muratov et al. (2015), which guided the current implementation of supernova feedback in SAG.

2.3 The sample of simulated backsplash galaxies, three stages, four types

Our study focuses on 34 massive, relaxed, and isolated galaxy clusters that were selected from the MDPL2-SAG galaxy catalogue. To identify these clusters, we first applied selection criteria based on the halo mass and the presence of nearby companion haloes. Specifically, we selected all haloes at redshift $z = 0$ with a mass $M_{200} \geq 10^{15} h^{-1} M_\odot$, and with no companion haloes within $5 \times R_{200}$ that are more massive than $0.1 \times M_{200}$. Here, M_{200} refers to the mass enclosed within a region of radius R_{200} that encompasses 200 times the critical density. These selection criteria were designed to exclude haloes that are undergoing major mergers or interacting with massive companions, which may have an impact on the orbits of galaxies in the vicinity of the clusters. This cluster sample is identical to the one employed in the works of de los Rios et al. (2021) and Coenda et al. (2022) for the development and testing of the ROGER code which dynamically classifies galaxies in and around clusters in the projected phase space. Throughout this paper we use galaxies with $M_\star \geq 3 \times 10^8 h^{-1} M_\odot$ since stellar mass functions and galaxy properties cannot be reliably replicated for galaxy masses lower than this threshold (Knebe et al. 2018).

We have adopted the same classification scheme as de los Rios et al. (2021) to categorize galaxies in and around the selected clusters based on their orbits. In particular, we define backsplash (BS) galaxies as those galaxies which at $z = 0$ are found outside R_{200} ,

¹ <https://www.cosmosim.org/cms/simulations/mdpl2/>

² <http://skiesanduniverses.org/Simulations/MultiDark/>

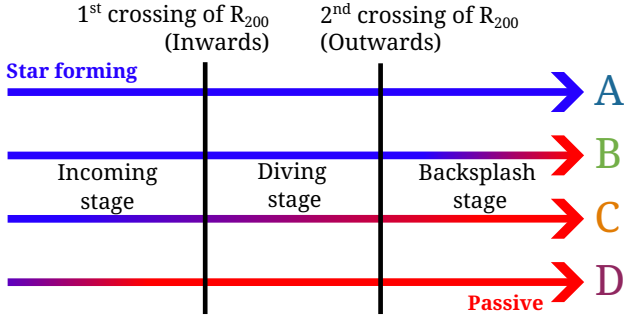


Figure 1. Scheme adopted for the selection of different types of BS galaxies based on the moment when a galaxy transitions from being star forming to a passive state. Blue colour symbolises a star forming galaxy, while red denotes a passive one. The four types of galaxies are: galaxies that never become passive (A); galaxies that become passive during their backsplash stage (B); galaxies that become passive while they are inside the cluster (C); galaxies that become passive before entering the cluster (D).

having crossed this radius exactly twice in their lifetimes, the first time on their way in, and the second on their way out of the cluster.

Hereafter, our paper will solely focus on the backsplash galaxies, and we will refer to them as BS galaxies to prevent confusion with the term *backsplash stage*, introduced below.

We follow the evolution of galaxies through three stages in their lifetimes:

- **Incoming stage:** the period of 2 Gyr preceding the first time a galaxy crosses R_{200} in an inward direction.
- **Diving stage:** the span of time the galaxy remains within R_{200} .
- **Backsplash stage:** the lapse of time between the moment when the galaxy crosses R_{200} for the second time in an outward direction, and the present epoch at $z = 0$.

Following the criterion adopted by Cora et al. (2018), galaxies with a specific star formation rate (sSFR) higher than $10^{-10.7} \text{ yr}^{-1}$ are defined as star forming, meanwhile galaxies with sSFR below that threshold are classified as passive. We have classified the galaxies into four distinct types based on whether they are star forming or passive at the different stages.

- **Type A:** galaxies that are star forming throughout the three stages; 3038 galaxies in total, 58 per cent of the sample.
- **Type B:** galaxies that become passive during their backsplash stage; 1353 galaxies, 26 per cent of the sample.
- **Type C:** galaxies that become passive during their diving stage; 200 galaxies, 4 per cent of the sample.
- **Type D:** galaxies that become passive prior to their diving stage, i.e. during the incoming stage or even before; 622 galaxies, 12 per cent of the sample.

This classification scheme is summarised in Fig. 1.

In Fig. 2, we show both the stellar mass distributions for the four types and for the total sample of BS galaxies at $z = 0$ (upper panel), and the fraction of galaxies of each type as a function of their stellar mass at $z = 0$ (bottom panel). There is no surprise in this plot. At the low-mass end ($M_{\star} \lesssim 10^{10} h^{-1} M_{\odot}$), the majority of galaxies are still star forming (type A). The fractions that follow in descending order correspond to galaxies that ceased star formation after leaving the cluster (type B). On the other hand, at the high-mass end ($M_{\star} \gtrsim 10^{11} h^{-1} M_{\odot}$), most of the galaxies were passive prior to diving into the cluster (type D). The tran-

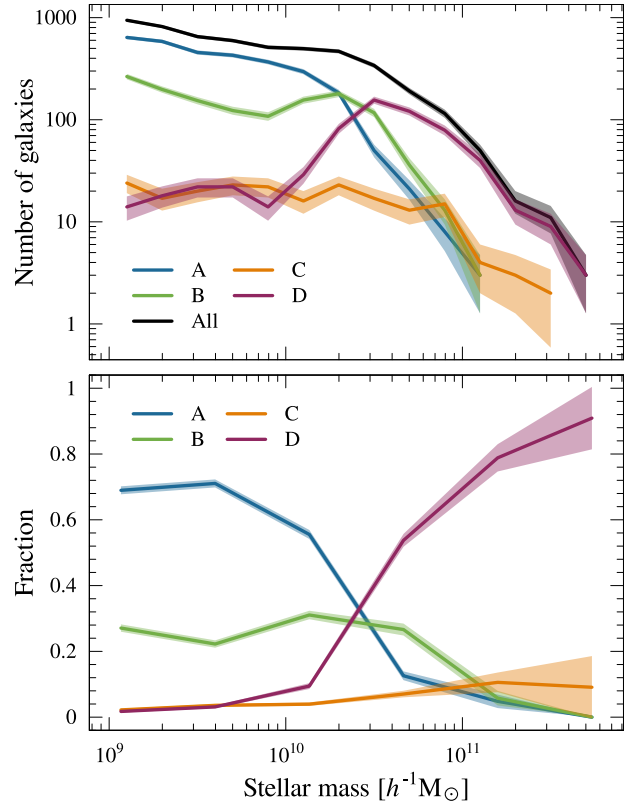


Figure 2. Upper panel: Stellar mass distributions for the four types (color lines) and for the complete sample (black line) of BS galaxies at $z = 0$. Shaded regions represent Poisson errors. Bottom panel: Fractions of the four galaxy types as a function of their stellar mass at $z = 0$. The median values are indicated by lines, while bootstrap errors are represented by shaded regions.

sition between these two regimes occurs at intermediate masses, $M_{\star} \sim 3 \times 10^{10} h^{-1} M_{\odot}$. The fraction of galaxies that became passive during their diving stage (type C) is very low over the whole range of mass, accounting only for 4 per cent of the complete sample of galaxies. This is an indication that the cluster environment can not easily quench a galaxy while diving though it for the first time. Nevertheless, about a quarter of all BS galaxies (~ 30 per cent of the galaxies that entered as star forming), become passive after leaving the cluster (Type B), which suggests that the effects of the cluster environment on the star formation of galaxies are not immediate and may take some time to manifest. Galaxies with stellar masses below the aforementioned transition value exhibit a clear manifestation of this phenomenon. To gain deeper insights into the underlying physical mechanisms responsible for the variation in the proportions of different galaxy types and their correlation with stellar mass, we analyse in detail the dynamics and astrophysical properties of these objects.

3 DYNAMICS

This section delves into the main aspects of the dynamics of BS galaxies, which comprises their entry and exit points from clusters, velocities, duration of the diving stage, and the proximity to the cluster centre at their pericentre. It is essential to consider not only

distances with respect to the centers of clusters but also directions in space concerning the main axes of the clusters. This approach is crucial for a comprehensive understanding of the spatial orientation of objects within the cluster environment. We determine the main axes of each cluster in our sample by diagonalising the cluster's shape tensor. For this purpose, we use the position of all galaxies whose dark matter haloes are subhaloes gravitationally bound to the main cluster halo as identified by ROCKSTAR at $z = 0$, that is satellite galaxies within dark matter substructures. The shape tensor is defined as:

$$S_{ij} = \sum_{k=1}^N X_k^i X_k^j, \quad (1)$$

where the dummy index k runs from 1 to the number of galaxies, N , and X_k^i and X_k^j are the i -axes and j -axes Cartesian coordinates of the galaxy k , respectively. By solving the eigenvalue problem of the shape tensor, we determine the direction of the orthogonal axes of symmetry of the galaxy distribution. The main axis will be the one along which the distribution of galaxies is most extended. The secondary and tertiary axes follow in decreasing elongation. We have computed the main axes of the clusters at many different outputs of the SAG model, and found that they are stable enough for our purposes in the last few Gyrs. Thus, for simplicity, we consider the main axes at $z = 0$ in our computations.

For each cluster we define a right hand rule Cartesian coordinate system where the X -axis, Y -axis and Z -axis are the main, secondary and tertiary axes, respectively. We define clustercentric angular positions relative to these axes taking as fundamental plane the $X - Y$ plane: the longitude $l \in [0^\circ, 360^\circ)$, and the latitude $b \in [-90^\circ, 90^\circ]$. We compute the angular position of each galaxy in our sample relative to its parent cluster and stack them all into a unique sample we use throughout the paper.

We show in Fig. 3 the stacked angular positions of galaxies when they enter their parent cluster and when they leave it (upper and lower panels, respectively). In both cases, there is a noticeable accumulation of galaxies around the primary axis. However, when galaxies enter the cluster, there appears to be a stronger concentration that tends to diffuse primarily over the $X - Y$ plane as they depart. To quantify this, we compute the angular overdensity of galaxies at the times they cross R_{200} ,

$$\Delta(\lambda, \beta) = \frac{N(\lambda, \beta)}{N_R(\lambda, \beta)} - 1, \quad (2)$$

by counting the number, $N(\lambda, \beta)$, of galaxies with angles

$$\lambda = \begin{cases} l, & \text{if } l \leq 90^\circ \\ |180^\circ - l|, & \text{if } 90^\circ < l < 270^\circ \\ 360^\circ - l, & \text{if } l \geq 270^\circ, \end{cases} \quad (3)$$

and

$$\beta = |b|. \quad (4)$$

These angles are the distance in longitude with respect to the cluster main axes, and the distance in latitude from the cluster main plane. $N_R(\lambda, \beta)$ is the expected number of points with angular coordinates (λ, β) in a homogeneous angular distribution over the sphere. To compute this number we generate a random distribution of angular points which covers the sphere homogeneously. This distribution contains 100 times the number of galaxies in the sample, therefore, $N_R(\lambda, \beta)$ is the number of these random points with coordinates (λ, β) divided by 100. In addition, we compute the overdensity of galaxies, $\omega(\theta)$, as a function of the angular distance to

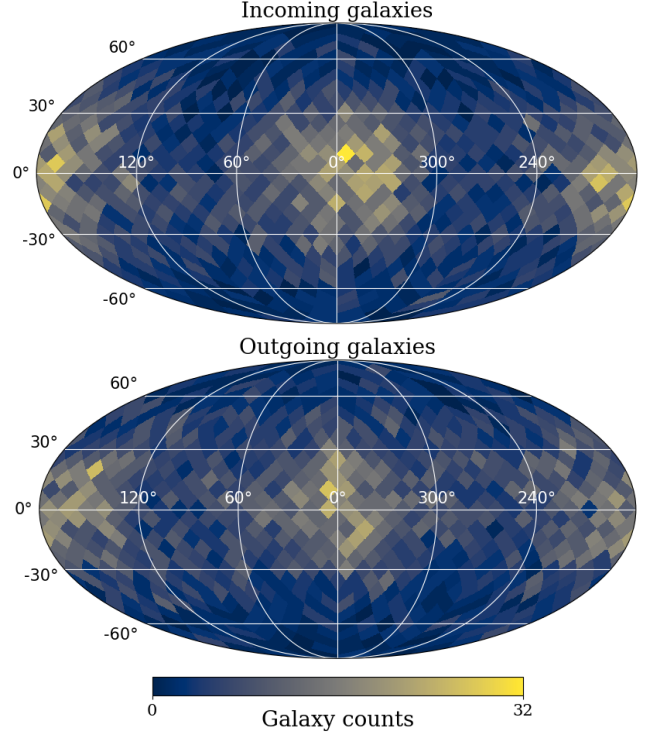


Figure 3. Mollweide projection of the angular distribution of galaxies relative to their parent cluster's main axes. *Upper panel:* the angular distribution of incoming galaxies at the moment they cross R_{200} of the cluster in an inward direction. *Lower panel:* the angular distribution of outgoing galaxies as they move away from the R_{200} boundary. In these plots, the coordinates of the main axis are $(l, b) = (0^\circ, 0^\circ)$, and $(180^\circ, 0^\circ)$; the secondary axis' coordinates are $(l, b) = (90^\circ, 0^\circ)$, and $(270^\circ, 0^\circ)$; the tertiary axis is located at latitude $b = -90^\circ$, and 90° .

the main axis, $\theta = \arccos(\cos(\beta)\cos(\lambda))$, which is computed in an analogous way as $\Delta(\lambda, \beta)$.

The results of the computation of the angular overdensity for the general population of galaxies are shown in Fig. 4. The left panel of this figure shows that the majority of galaxies tend to enter the cluster within a range of $\sim 35^\circ$ of the plane, with some entering up to $\sim 50^\circ$ in longitude; a strong concentration is observed towards the primary axis itself. The overdensity isocontours are found to extend farther in longitude than in latitude, with a difference of a factor ~ 2 for the two highest value isocontours shown ($\Delta = 1$, and 1.5). For outgoing galaxies (central panel), changes in the shape of the isocontours are observed, with the highest overdensity isocontours ($\Delta \geq 0.5$) appearing to shrink. However, the overall overdensity enclosed by the $\Delta = 0$ isocontour is found to extend further over the main plane, with a range of up to $\lambda \sim 60^\circ$. The majority of galaxies tend to enter the cluster near the primary axis and over the main plane, and to exit the cluster over the same plane, albeit with less concentration towards the primary axis. The right panel of Fig. 4 reinforces this behaviour: while the overdensities of both incoming and outgoing galaxies are seen at angular scales of $\theta \lesssim 50^\circ$, the overdensities of incoming galaxies are systematically greater over that range. This deflection is in qualitative agreement with the results by Kuchner et al. (2022) where the authors suggest that BS entering through a filament do not necessarily return along a filament.

We perform the same analysis for the subsamples of galaxies

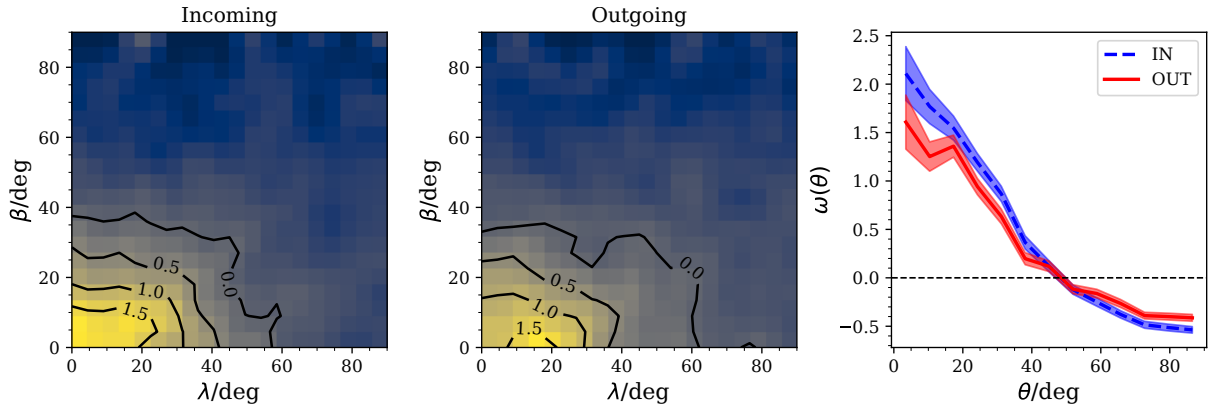


Figure 4. Angular overdensity of galaxies relative to their parent cluster’s main axes. *Left panel:* overdensity of incoming galaxies as they enter R_{200} as a function of the distance in longitude with respect to the primary axis, λ , and the absolute value of latitude, β . In this plot, the primary axis of the cluster has coordinates $(\lambda, \beta) = (0^\circ, 0^\circ)$, the secondary $(\lambda, \beta) = (90^\circ, 0^\circ)$, and the tertiary $\beta = 90^\circ$. Some relevant isocontours are drawn in solid line. *Middle panel:* same as the *left panel* but for outgoing galaxies. *Right panel:* the angular overdensity of incoming (IN) and outgoing (OUT) galaxies as a function of the angular distance, θ , to the primary cluster axis. Errors are computed using the bootstrap resampling technique.

of different type, as defined in the previous section. This is shown in Fig. 5. Each row in this figure considers a different galaxy type, from A to D, moving from top to bottom respectively. Comprising 58 per cent of the total sample, type A galaxies show angular overdensities that resemble those of the entire sample, i.e., they are mildly deflected over the main plane. Type B galaxies constitute the most interesting case, as they also display deflections over the main plane, but their trajectory out of the cluster systematically deviates from the primary axis. This is further highlighted by the characteristics exhibited in the angular overdensity $\omega(\theta)$: outgoing type B galaxies present a broad peak at $15^\circ \lesssim \theta \lesssim 35^\circ$, and a sharp decline towards $\theta = 0^\circ$. This strong deflection is not seen for the other three types. Finally, the less numerous type C and D galaxies seem to get in and out the cluster much more closer to the primary axis, as if they were accreted into the cluster by inner regions of filaments and expelled out the cluster in a similar way (González & Padilla 2016; Salerno et al. 2019, 2020; Morinaga & Ishiyama 2020). This is consistent with the definition of these two types, they are either already quenched when they enter the cluster, or are quenched in their incursion through it.

Other dynamical parameters are shown in Fig. 6, namely: incoming velocity, the distance of the pericentre, the timespan of the diving stage, the ratio between the incoming and the outgoing velocities, and the timespan of the backsplash stage. All these parameters are shown as median values per type, as a function of stellar mass (left panels), and as a single value stacking all galaxies together regardless of their mass (right panel). It is evident from the left panels that there are no notable patterns between these parameters and stellar mass and, also, it is fair to notice the lack of some types of galaxies for stellar masses higher than $\sim 7 \times 10^{10} h^{-1} M_\odot$, where a complete comparison can not be done.

Regarding the incoming velocity (top panels), it seems that Type C galaxies have a tendency to enter clusters at lower velocities compared to the other types, whereas no discernible difference is observed among types A, B, and D. Instead, in the case of pericentre distance (shown in the second panel from the top), type A galaxies stand out, as they exhibit systematically larger distances from the cluster centre at their closest point to it than the other galaxy types. On the other hand, there are no significant differences among the other types. When analysing how long galaxies are inside R_{200} (middle panels), we find that types A and D cannot be

distinguished, but type B spends the least amount of time, while on the opposite end, type C remains for the longest duration. There is no difference among the four types with regards to the ratio between the outgoing and incoming velocities (second panel from the bottom). All types get out the cluster at speeds ~ 20 per cent lower than they had when they entered the cluster. Finally, type B galaxies are the ones that have spent the longest time in the backplash stage, while no differences are seen among the other types (bottom panel).

We have checked that 27 per cent of the complete sample of BS galaxies are falling back to the cluster at $z = 0$, and this fraction does not vary significantly with the galaxy type. The only exception are type B galaxies for which this percentage increases to 38, in consistency with the fact that they spend typically longer times in the backplash stage.

4 THE PHYSICAL EVOLUTION OF BACKSPLASH GALAXIES

In this section we study how physical properties of MDPL2-SAG BS galaxies evolve in the three stages. We focus on some quantities provided by the SAG model: stellar mass, dark matter halo mass, cold gas mass, hot gas mass, and the specific star formation rate. Towards the end of this section, we examine morphological changes experienced by these galaxies by using the ratio of bulge mass to total stellar mass as a proxy of morphology.

4.1 Astrophysical quantities

The evolution of astrophysical properties of BS galaxies is presented in Fig. 7. As temporal variable we use τ , defined as the time a galaxy remains in a particular stage conveniently normalised. For the incoming stage, we considered as $\tau = 0$ to 2 Gyr before the galaxy crosses R_{200} inwards the cluster, and $\tau = 1$ as the moment when the galaxy crosses R_{200} for the first time. For the diving stage, $\tau = 0$ is set at the moment the galaxy crosses R_{200} inwards the cluster and $\tau = 1$ when the galaxy crosses R_{200} outwards. Finally, in the backplash stage, we define as $\tau = 0$ the time the galaxy crosses R_{200} for the second time and $\tau = 1$ corresponds to $z = 0$. With this

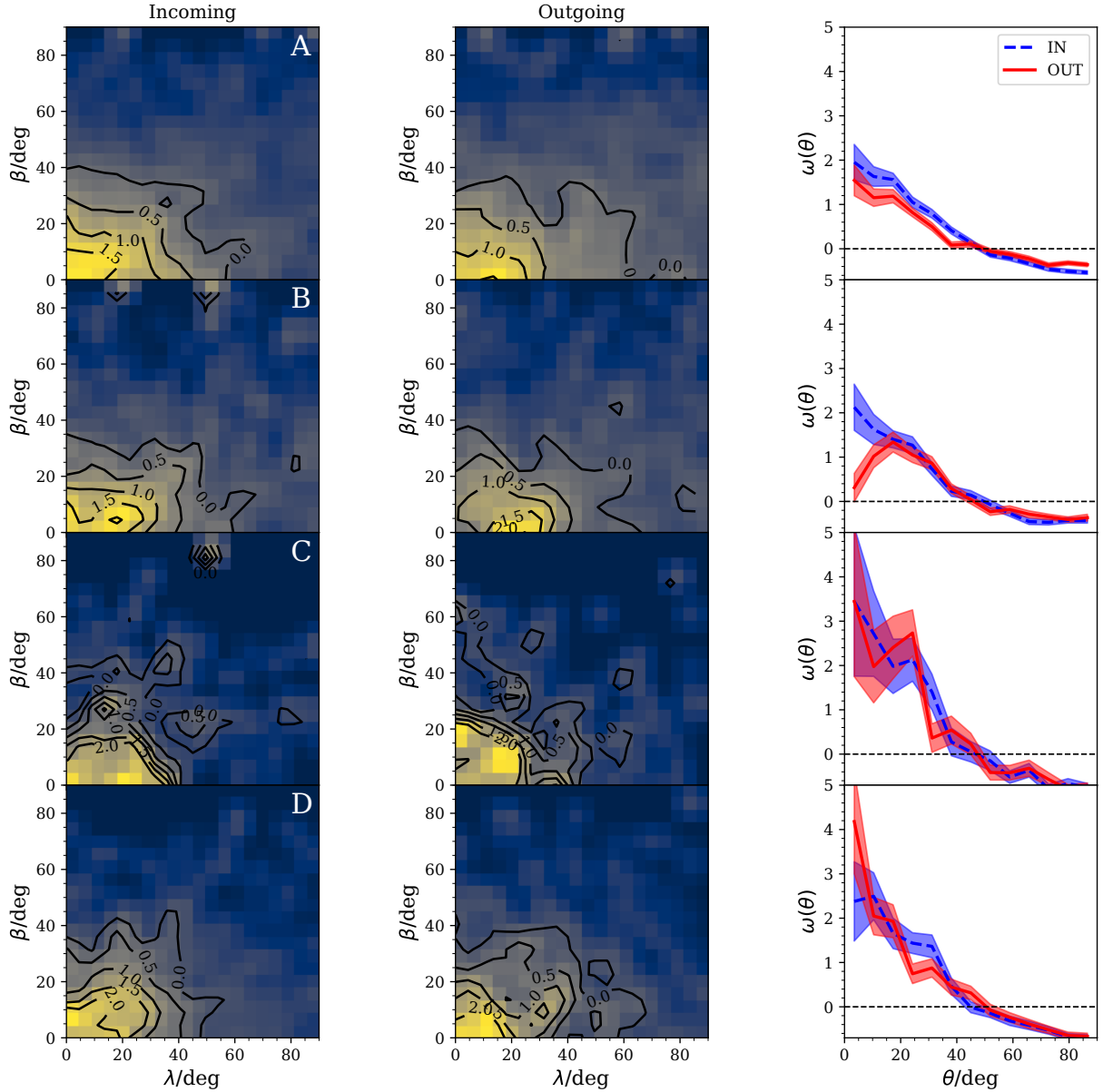


Figure 5. Same as Fig. 4 but considering each of the four types of galaxies separately as quoted in left panels.

normalised time, we stacked the evolution of astrophysical properties normalised to their values at a particular moment τ_* : this τ_* is the first crossing of R_{200} for incoming and diving stages, and corresponds to the second crossing of R_{200} for the backsplash stage. All these time definitions are shown at the bottom panels of the figure. From top to bottom in Fig. 7, the properties shown are: stellar mass, dark matter halo mass, cold gas mass, hot gas mass, and specific star formation rate. In all cases, we show the median values of the evolution of the stacked galaxy population with errorbars (shaded regions) computed with a bootstrap resampling.

We begin our analysis by studying the total stellar mass of galaxies. Type A galaxies exhibit the most substantial increase in their stellar masses across the three stages: approximately 20 per cent during the incoming stage, 10 per cent during the diving stage, and 5 per cent during the backsplash stage. Type B galaxies show a similar trend during the first two stages, but their median growth in stellar mass halts during the backsplash stage. This outcome is

anticipated since, by definition, these galaxies become passive during this stage. In the case of types C and D galaxies, only type C galaxies exhibit a marginal increase of ~ 5 per cent in their masses during the incoming stage. These behaviours are consistent with our classification: galaxies that become passive at a later stage exhibit a correspondingly delayed decrease in the median stellar mass growth.

The evolution of the mass of the dark matter halo where the galaxy resides is completely determined by the dynamical interactions of the haloes across their merger trees histories. As can be seen in the second row of panels from Fig. 7, for all galaxy types, the host haloes decrease in mass across the three stages. In the incoming stage, haloes of type C galaxies are the most affected, losing up to ~ 20 per cent of their mass. Similarly, the diving stage causes a more significant impact on the haloes of type C galaxies (~ 40 per cent), whereas the haloes of the remaining types experience losses of around 20 per cent. The fact that type

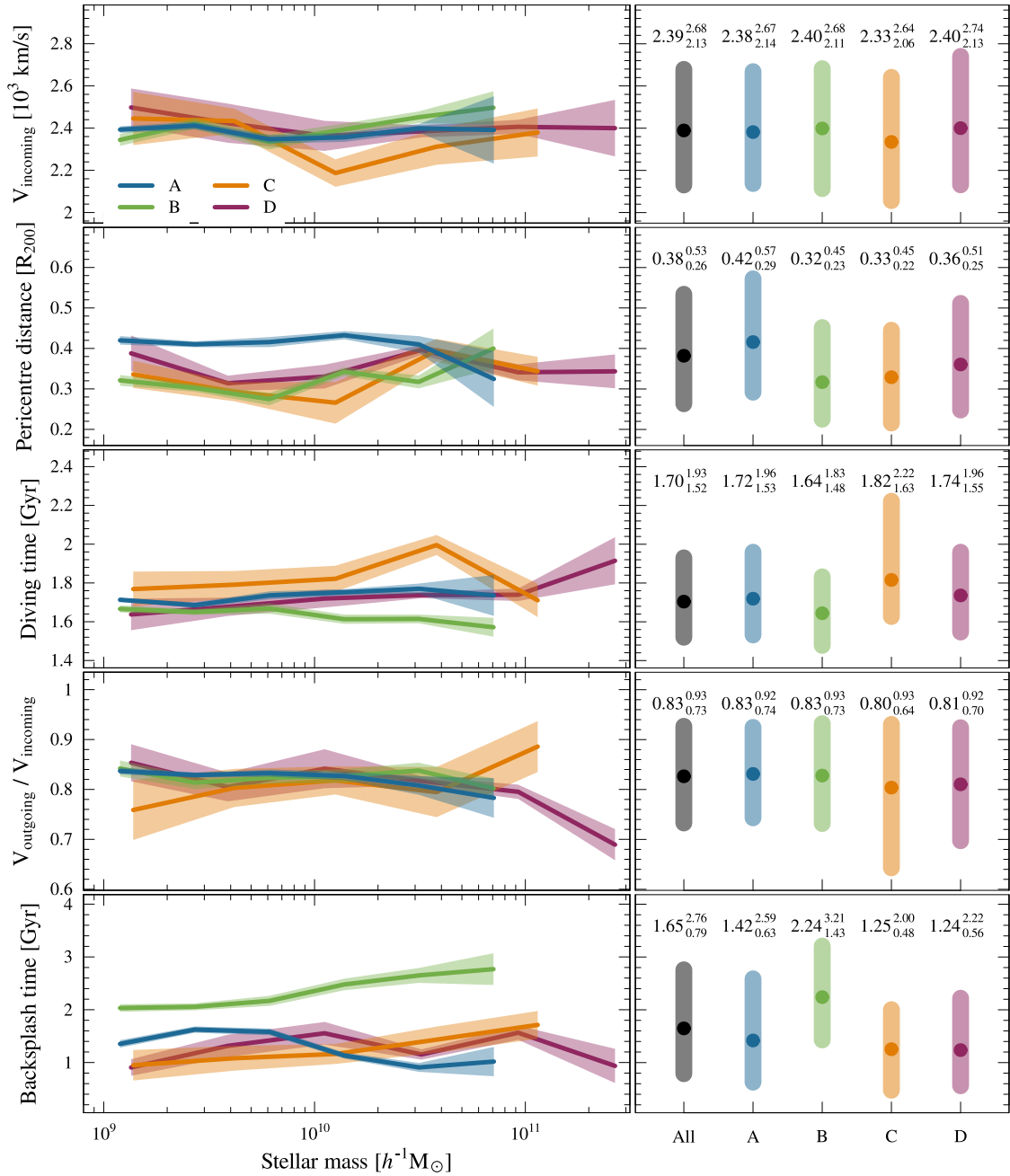


Figure 6. *Left panels:* Dependence of several dynamical properties with stellar mass for the four types of galaxies. From top to bottom: incoming velocity modulus, normalized pericentre distance, time in the diving stage, ratio between outgoing and incoming velocity modulus and time in the backplash stage. In all cases we show the median value and the errors computed with bootstrap resampling. *Right panels:* Median values (central dot) and quartiles (shaded bars) for the same properties described in left panels. Numerical values are quoted for each type, including the complete sample of galaxies.

C galaxies become passive during the diving stage may be correlated with the significant mass disruption experienced by their host haloes during this stage. This tidal stripping of their haloes exposes them to a stronger effect of the ram pressure upon their hot gas (see Vega-Martínez et al. 2022 for details of the implementation of these processes in sag). Furthermore, these galaxies endured heavy pre-processing in the incoming stage. During the backplash stage, haloes of type B galaxies are those that experience the greatest impact on their masses, with a decrease of over ~ 40 per cent. Nevertheless, haloes of the other galaxy types also show a reduction of ~ 30 per cent in their masses at $z = 0$. Once again, we notice a

correlation between the haloes that suffer the most significant mass loss and the fact that the galaxies inhabiting them (type B) become passive during this stage. This finding is consistent with their null stellar mass growth. It is worth noting that, during the backplash stage, all galaxies except for type A have ceased to grow their stellar mass, and the dark matter haloes continue to shrink across all classifications.

In the third and fourth rows of panels of Fig. 7, we show the evolution of the cold and hot gas mass, respectively. Type A galaxies do not undergo significant changes in their cold and hot gas masses during the incoming stage, but suffer a reduction of ~ 20

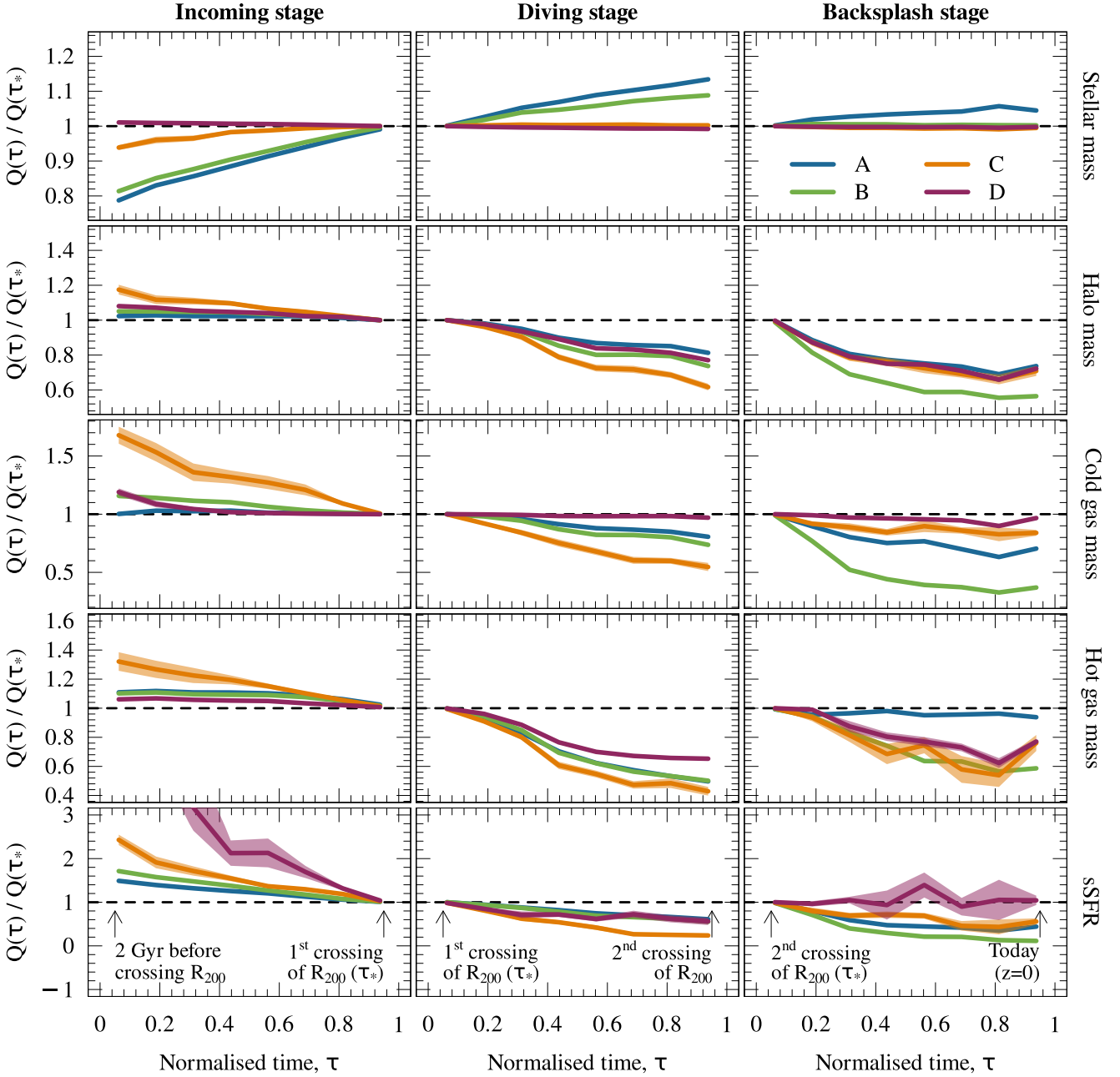


Figure 7. Evolution of normalised astrophysical properties for the four types of galaxies in the three stages. Evolution is parameterized with τ , a normalized time at two particular moments in each stage, as indicated with arrows at the bottom panels. The astrophysical properties are normalised at their values at τ_* , which is the first crossing of R_{200} for the incoming and diving stages, and the second crossing of R_{200} for the backsplash stage. Properties Q are, from top to bottom, the stellar mass, the dark matter halo mass, the mass in cold gas, the mass in hot gas and the specific star formation rate. In all cases, we show the median of the stacked galaxy population and errorbars computed via bootstrap resampling.

per cent of the cold gas and ~ 50 per cent of the hot gas when they are located inside the R_{200} radius of the cluster. Once they are out, in the backsplash stage, they continue losing cold gas (~ 30 per cent) but the amount of hot gas remains stable. This may be explained by the negligible effect of the RP on these galaxies due to their greater distance from the cluster. Type B galaxies lose more than 50 per cent of their cold gas during the backsplash stage, period where these galaxies become passive. They also get their hot

gas drastically removed in the diving (~ 50 per cent) and backsplash (~ 40 per cent) stages. Notably, the difference between type B and type A galaxies is that in the backsplash stage, type B galaxies experience a considerable removal of hot gas, while type A galaxies retain their hot gas. This difference explains why type B galaxies become passive during the backsplash stage. In the incoming stage, type C galaxies suffer a large reduction of ~ 70 per cent in their cold gas mass, which continues during the diving stage, reaching

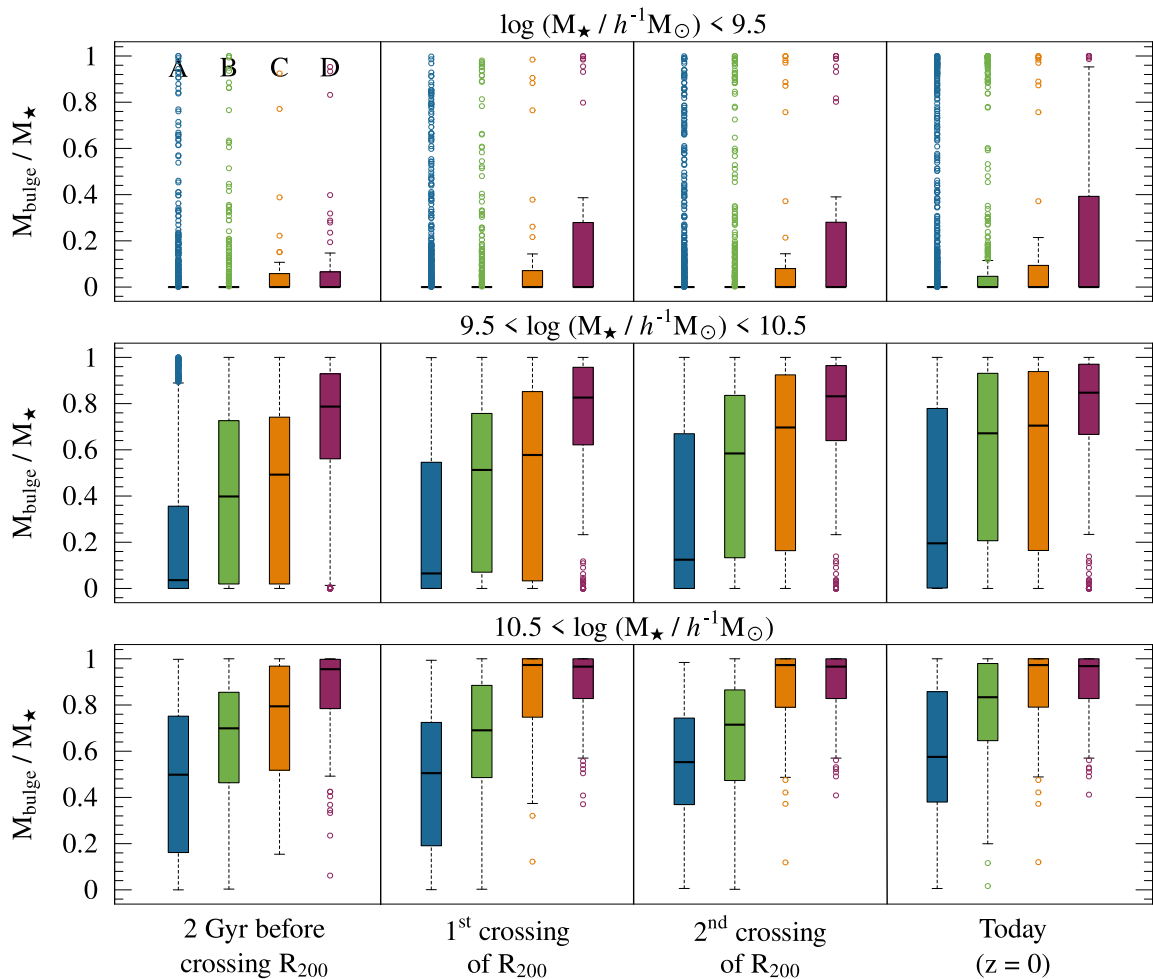


Figure 8. Boxplots for morphological distributions for the four galaxy types, where morphology is defined as the ratio between the bulge mass and the total stellar mass, $M_{\text{bulge}}/M_{\star}$. Distributions are shown for three stellar mass cuts, from low-mass galaxies (top) to high-mass galaxies (bottom), and at four different moments in the galaxy lifetime, as indicated in the x-axis labels. In each boxplot, the color bar represent the interquartile range $IQR = Q_3 - Q_1$, where Q_1 and Q_3 are the first and third quartiles of the distribution, respectively, and the median value is shown with the short horizontal black line. The dashed vertical lines show the range covered by the minimum and maximum values, without considering the outliers of the distribution, which are defined as those at a distance greater than $1.5 \times IQR$ of Q_1 or Q_3 and symbolized with the coloured open circles.

another reduction of ~ 50 per cent at the time the galaxy leaves the cluster. The same occurs with hot gas, suffering reductions of ~ 30 , 60 and 40 per cent during the incoming, diving and backsplash stages, respectively. Type D galaxies exhibit a notable change in their cold gas content only during the initial phase of the incoming stage which is in line with their quenched state upon entering the cluster. At this point, the cold gas is neither consumed by star formation nor removed by RPS, as these galaxies still possess a hot gas shield that is gradually stripped away, reaching a loss of ~ 35 per cent in the diving and backsplash stages.

Finally, in the last row we show the sSFR. While all galaxy types exhibit a decrease in their sSFR throughout all stages, it is evident that type D galaxies, which are already passive upon infalling into the cluster, are highly affected during the incoming stage. These galaxies experience a further decrease in their sSFR during the diving stage and maintain a stable sSFR during the back-splash stage. Type C galaxies also experience a significant drop in their sSFR during the incoming stage, and they are the most affected among all types in the diving stage, losing nearly all their

ability to form stars. During the incoming and diving stages, types A and B exhibit similar trends by reducing their sSFR by ~ 50 . However, in the backsplash stage, type B galaxies become passive and experience the most significant decrease in sSFR.

4.2 Morphology

The overall analysis of the sSFR fails to distinguish between the two modes of star formation: quiescent and bursty. In the context of SAG, generally considered in galaxy formation models, quiescent star formation contributes to the creation of the stellar disc, while bursty star formation, triggered by mergers and disc instabilities, leads to the formation of the stellar bulge. The proportion of the galaxy's total stellar mass that the bulge represents is an indicator of the galaxy's morphology.

In this section we analyse how the morphology of galaxies evolves across the three stages. To do this, we define as a proxy of the morphology the ratio of the bulge mass to the total stellar mass, $M_{\text{bulge}}/M_{\star}$. This ratio ranges between 0 for irregular galaxies (no

bulge mass) to 1 for elliptical galaxies (no disc mass), with spiral galaxies between those two extreme values.

In Fig. 8 we present boxplots for morphology distributions at four fixed times, from left to right: 2 Gyr before the galaxy crosses R_{200} for the first time, the moment when the galaxy crosses R_{200} inwards, the moment when the galaxy crosses R_{200} outwards and the present time ($z = 0$). Also, we divide the samples of galaxy types into three stellar mass ranges, from top to bottom: $\log(M_{\star}/h^{-1}M_{\odot}) < 9.5$ (low mass), $9.5 < \log(M_{\star}/h^{-1}M_{\odot}) < 10.5$ (intermediate mass) and $10.5 < \log(M_{\star}/h^{-1}M_{\odot})$ (high mass).

The first feature easily noticeable is that, at early times, low-mass galaxies (top panels) mostly have $M_{\text{bulge}}/M_{\star} \sim 0$, which does not change significantly across the galaxy lifetime. In particular, types A and B populations are highly dominated by bulgeless galaxies, which represent 90, 84, 81 and 79 per cent of the sample for type A, and 85, 79, 75 and 71 per cent of the sample for type B, at each of the moments considered along the galaxy lifetime. Only type D galaxies show a mild evolution in their morphology, specially between the 2 Gyr before of entering the cluster and the moment galaxies crosses R_{200} for the first time, that is, during the incoming stage. For intermediate and high stellar masses (middle and bottom panels, respectively), we can appreciate a smooth morphological change across cosmic time for all galaxy types.

These results show that the morphological evolution of galaxies is a smooth and continuous process during the stages defined in this work. We do not find evidence that a particular moment in the lifetime of BS galaxies can induce a major morphological transformation, in agreement with Martínez et al. (2023), where the authors find evidence that quenching occurs faster than morphological transformation for galaxies around massive X-ray clusters as classified with ROGER (de los Rios et al. 2021). We only find a clear dependence of morphology with the stellar mass cuts analysed, dependence that is also manifested through the relationship between the galaxy type and its stellar mass (see Fig. 2). At this point, it is worth recalling that larger stellar masses correlate with larger bulge masses, and this implies the existence of larger black holes in those galaxies (McConnell & Ma 2013; Kormendy & Ho 2013; Schutte et al. 2019). These massive black holes bring with an associated major feedback from active galactic nuclei that accelerates the quenching processes, specially for types C and D.

5 CONCLUSIONS

In this paper we have studied the population of BS galaxies around a sample of massive, isolated clusters at $z = 0$ in the MDPL2-SAG catalogue of simulated galaxies. It is important to recall that our definition of BS galaxy involves a single passage within R_{200} , thus these galaxies experience the environmental action of the cluster only in this single passage. The main focus of this paper is to understand what happens to a galaxy that passes only once through a cluster, and not the cumulative effect of several orbits inside the cluster. We classified the BS galaxies into four types based on their star-forming or passive nature at three different stages: incoming stage, diving stage, and backplash stage. We analysed various dynamical and astrophysical properties of these galaxies.

For galaxies that are actively forming stars at all stages (type A), we find they typically have stellar masses below $3 \times 10^{10} h^{-1} M_{\odot}$ at $z = 0$. Due to their orbits avoiding the innermost regions of the cluster, their incursion into the cluster has minimal impact on them. Consequently, they do not experience significant losses in their dark matter or gas contents, allowing them to continue forming stars.

We find that BS galaxies that become passive during the backplash stage (type B) also have masses typically below $3 \times 10^{10} h^{-1} M_{\odot}$ at $z = 0$, similarly to type A galaxies. They constitute the vast majority of passive BS galaxies in that mass range. Their orbits inside the cluster are characterised by the smallest pericentric distances of all four types, and, on average they experience a strong deflection away from the primary axes in their way out. This close encounter with the centre of the cluster it is the single most important factor in the subsequent evolution of these galaxies. The action of the cluster leaves its mark in the strong loss of these galaxies' dark matter and gas contents, and the subsequent suppression of their star formation in the backplash stage. Had these galaxies not come that close to the centre, they would probably have been classified as Type A. This galaxy population can be associated to the low mass galaxies quenched after their first passage through the pericenter in massive clusters described by Wright et al. (2022) using the EAGLE simulations (Schaye et al. 2015; Crain et al. 2015).

Regarding those galaxies that become passive during the diving stage (type C), they are the least abundant among all BS. They entered the cluster in close proximity to the primary axes and underwent significant pre-processing. Among the galaxies that enter the cluster while still forming stars, these galaxies are the ones that remain for the longest duration and endure the greatest reductions in their dark matter and gas contents in the incoming stage. The cluster then provides the final blow to these galaxies' star formation.

Finally, galaxies that are passive throughout the three stages (type D) are typically high mass galaxies that were quenched before entering the cluster. Typically, they are accreted close to the primary axes, and get out the cluster along the same axes. There is nothing particularly noteworthy about these galaxies after they dive into the cluster.

Our results are in agreement with those presented by Hough et al. (2023), where the authors show that 65 per cent of present day star-forming BS galaxies did not experience pre-processing effects before their passage to the pericentre. On the other hand, 70 per cent of $z = 0$ quenched galaxies suffer larger removals of hot gas during their pre-processing instances (incoming stage) and inside the cluster (diving stage). These quenched BS galaxies can be clearly related with our D and C types, respectively. It is important to mention that the authors define as BS a galaxy that is outside R_{200} at $z = 0$ but have been inside the cluster at least once in the past, which is slightly different than our definition, where we allow just one passage to the pericentre. This difference implies some of their BS galaxies should be more quenched than ours as they have suffered the action of the cluster in more than one passage.

Regarding morphology, a consistent pattern is observed across the four types: a single passage through the cluster does not generally induce significant morphological transformations, as suggested by Martínez et al. (2023). It should be kept in mind that we are using a proxy for morphology and not a precise characterisation of it.

The main result of this paper is that the environmental effects of the cluster is able to affect galaxies after a single passage provided they are either: low-intermediate mass ($< 3 \times 10^{10} h^{-1} M_{\odot}$) galaxies whose orbits take them very close to the centre, or galaxies that entered the cluster heavily pre-processed. The former stop forming stars after exiting the cluster, while the latter do so in situ.

ACKNOWLEDGEMENTS

We kindly thank the anonymous Referee for comments and suggestions that improved the original manuscript. This paper has been partially supported with grants from Consejo Nacional de Investigaciones Científicas y Técnicas (PIPs 11220130100365CO, 11220210100064CO and 11220200102832CO) Argentina, the Agencia Nacional de Promoción Científica y Tecnológica (PICTs 2020-3690 and 2021-I-A-00700), Argentina, and Secretaría de Ciencia y Tecnología, Universidad Nacional de Córdoba, Argentina. ANR thanks the Scaloneta for winning the 2022 FIFA World Cup. MDIR acknowledges financial support from the Comunidad Autónoma de Madrid through the grant SI2/PBG/2020-00005. The COSMOSIM database used in this paper is a service by the Leibniz-Institute for Astrophysics Potsdam (AIP). The MULTIDARK database was developed in cooperation with the Spanish MultiDark Consolider Project CSD2009-00064. The authors gratefully acknowledge the Gauss Centre for Supercomputing e.V. (www.gauss-centre.eu) and the Partnership for Advanced Supercomputing in Europe (PRACE, www.prace-ri.eu) for funding the MULTIDARK simulation project by providing computing time on the GCS Supercomputer SuperMUC at Leibniz Supercomputing Centre (LRZ, www.lrz.de). All analyses in this paper have been done using the FORTRAN language (<https://fortran-lang.org>), and figures have been developed using R (R Core Team 2021), MATPLOTLIB (Hunter 2007), HEALPIX / HEALPY (Górski et al. 2005; Zonca et al. 2019) and INKSCAPE (<https://inkscape.org>).

DATA AVAILABILITY

The raw data of the semi-analytic model of galaxy formation SAG will be shared on reasonable request to the corresponding author.

REFERENCES

- Abadi M. G., Moore B., Bower R. G., 1999, *MNRAS*, **308**, 947
 Adami C., Biviano A., Mazure A., 1998, *A&A*, **331**, 439
 Aguerri J. A. L., Sánchez-Janssen R., 2010, *A&A*, **521**, A28
 Bahé Y. M., McCarthy I. G., Balogh M. L., Font A. S., 2013, *MNRAS*, **430**, 3017
 Balogh M. L., Navarro J. F., Morris S. L., 2000, *ApJ*, **540**, 113
 Bamford S. P., et al., 2009, *MNRAS*, **393**, 1324
 Barnes J. E., 1992, *ApJ*, **393**, 484
 Behroozi P. S., Wechsler R. H., Wu H.-Y., 2013a, *ApJ*, **762**, 109
 Behroozi P. S., Wechsler R. H., Busha M. T., Klypin A. A., Primack J. R., 2013b, *ApJ*, **763**, 18
 Behroozi P. S., Wechsler R. H., Lu Y., Hahn O., Busha M. T., Klypin A., Primack J. R., 2014, *ApJ*, **787**, 156
 Bekki K., 2009, *MNRAS*, **399**, 2221
 Benavides J. A., et al., 2021, *Nature Astronomy*, **5**, 1255
 Berrier J. C., Stewart K. R., Bullock J. S., Purcell C. W., Barton E. J., Wechsler R. H., 2009, *ApJ*, **690**, 1292
 Blanton M. R., Moustakas J., 2009, *ARA&A*, **47**, 159
 Blanton M. R., Eisenstein D., Hogg D. W., Schlegel D. J., Brinkmann J., 2005, *ApJ*, **629**, 143
 Book L. G., Benson A. J., 2010, *ApJ*, **716**, 810
 Borrow J., Vogelsberger M., O’Neil S., McDonald M. A., Smith A., 2023, *MNRAS*, **520**, 649
 Bower R. G., Benson A. J., Crain R. A., 2012, *MNRAS*, **422**, 2816
 Casey K. J., Greco J. P., Peter A. H. G., Davis A. B., 2023, *MNRAS*,
 Christensen C. R., Davé R., Governato F., Pontzen A., Brooks A., Munshi F., Quinn T., Wadsley J., 2016, *ApJ*, **824**, 57
 Cimatti A., et al., 2013, *ApJL*, **779**, L13
 Coenda V., Muriel H., Donzelli C. J., Quintana H., Infante L., García Lambas D., 2006, *AJ*, **131**, 1989
 Coenda V., Mast D., Martínez H. J., Muriel H., Merchán M. E., 2019, *A&A*, **621**, A98
 Coenda V., de los Ríos M., Muriel H., Cora S. A., Martínez H. J., Ruiz A. N., Vega-Martínez C. A., 2022, *MNRAS*, **510**, 1934
 Colberg J. M., White S. D. M., Jenkins A., Pearce F. R., 1999, *MNRAS*, **308**, 593
 Cooper M. C., Gallazzi A., Newman J. A., Yan R., 2010, *MNRAS*, **402**, 1942
 Cora S. A., et al., 2018, *MNRAS*, **479**, 2
 Crain R. A., et al., 2015, *MNRAS*, **450**, 1937
 Cui W., et al., 2018, *MNRAS*, **480**, 2898
 Dalla Vecchia C., Schaye J., 2008, *MNRAS*, **387**, 1431
 De Lucia G., Weinmann S., Poggianti B. M., Aragón-Salamanca A., Zaritsky D., 2012, *MNRAS*, **423**, 1277
 Delfino F. M., Scóccola C. G., Cora S. A., Vega-Martínez C. A., Gargiulo I. D., 2022, *MNRAS*, **510**, 2900
 Di Matteo P., Combes F., Melchior A. L., Semelin B., 2007, *A&A*, **468**, 61
 Domínguez M., Muriel H., Lambas D. G., 2001, *AJ*, **121**, 1266
 Dressler A., 1980, *ApJ*, **236**, 351
 Ebeling H., Barrett E., Donovan D., 2004, *ApJL*, **609**, L49
 Fujita Y., 2004, *PASJ*, **56**, 29
 Gill S. P. D., Knebe A., Gibson B. K., 2005, *MNRAS*, **356**, 1327
 Gnedin O. Y., 2003a, *ApJ*, **582**, 141
 Gnedin O. Y., 2003b, *ApJ*, **589**, 752
 González R. E., Padilla N. D., 2016, *ApJ*, **829**, 58
 Górski K. M., Hivon E., Banday A. J., Wandelt B. D., Hansen F. K., Reinecke M., Bartelmann M., 2005, *ApJ*, **622**, 759
 Gunn J. E., Gott J. R. I., 1972, *ApJ*, **176**, 1
 Haggard R., Gray M. E., Pearce F. R., Knebe A., Cui W., Mostoghiu R., Yepes G., 2020, *MNRAS*, **492**, 6074
 Hashimoto Y., Oemler Augustus J., Lin H., Tucker D. L., 1998, *ApJ*, **499**, 589
 Hasinger G., 2008, *A&A*, **490**, 905
 Hopkins P. F., Quataert E., Murray N., 2012, *MNRAS*, **421**, 3522
 Hou A., Parker L. C., Harris W. E., 2014, *MNRAS*, **442**, 406
 Hough T., et al., 2023, *MNRAS*, **518**, 2398
 Hunter J. D., 2007, *Computing in Science & Engineering*, **9**, 90
 Jackson R. A., Kaviraj S., Martin G., Devriendt J. E. G., Noakes-Kettel E. A., Silk J., Ogle P., Dubois Y., 2022, *MNRAS*, **511**, 607
 Klypin A., Yepes G., Gottlöber S., Prada F., Heß S., 2016, *MNRAS*, **457**, 4340
 Knebe A., et al., 2018, *MNRAS*, **474**, 5206
 Knebe A., et al., 2020, *MNRAS*, **495**, 3002
 Korzendy J., Ho L. C., 2013, *ARA&A*, **51**, 511
 Kuchner U., et al., 2022, *MNRAS*, **510**, 581
 Larson R. B., Tinsley B. M., Caldwell C. N., 1980, *ApJ*, **237**, 692
 Lu T., Gilbank D. G., McGee S. L., Balogh M. L., Gallagher S., 2012, *MNRAS*, **420**, 126
 Mamon G. A., Sanchis T., Salvador-Solé E., Solanes J. M., 2004, *A&A*, **414**, 445
 Marinacci F., et al., 2018, *MNRAS*, **480**, 5113
 Martín G., Kaviraj S., Devriendt J. E. G., Dubois Y., Pichon C., 2018, *MNRAS*, **480**, 2266
 Martínez H. J., Muriel H., 2006, *MNRAS*, **370**, 1003
 Martínez H. J., Coenda V., Muriel H., 2008, *MNRAS*, **391**, 585
 Martínez H. J., Muriel H., Coenda V., 2016, *MNRAS*, **455**, 127
 Martínez H. J., Coenda V., Muriel H., de los Ríos M., Ruiz A. N., 2023, *MNRAS*, **519**, 4360
 Mateus A., Sodré L., 2004, *MNRAS*, **349**, 1251
 McCarthy I. G., Frenk C. S., Font A. S., Lacey C. G., Bower R. G., Mitchell N. L., Balogh M. L., Theuns T., 2008, *MNRAS*, **383**, 593
 McConnell N. J., Ma C.-P., 2013, *ApJ*, **764**, 184
 McGee S. L., Balogh M. L., Bower R. G., Font A. S., McCarthy I. G., 2009, *MNRAS*, **400**, 937

- Mihos J. C., 2004, Cambridge: Cambridge Univ. Press, ed. J. S. Mulchaey, A. Dressler, & A. Oemler, p. 277
- Moore B., Katz N., Lake G., Dressler A., Oemler A., 1996, *Nature*, **379**, 613
- Moore B., Lake G., Katz N., 1998, *ApJ*, **495**, 139
- Morinaga Y., Ishiyama T., 2020, *MNRAS*, **495**, 502
- Muratov A. L., Kereš D., Faucher-Giguère C.-A., Hopkins P. F., Quataert E., Murray N., 2015, *MNRAS*, **454**, 2691
- Muriel H., Coenda V., 2014, *A&A*, **564**, A85
- Naiman J. P., et al., 2018, *MNRAS*, **477**, 1206
- Nandra K., et al., 2007, *ApJL*, **660**, L11
- Navarro J. F., White S. D. M., 1994, *MNRAS*, **267**, 401
- Nelson D., et al., 2018, *MNRAS*, **475**, 624
- Paulino-Afonso A., et al., 2019, *A&A*, **630**, A57
- Pillepich A., et al., 2018, *MNRAS*, **475**, 648
- Planck Collaboration et al., 2014, *A&A*, **571**, A16
- Planck Collaboration et al., 2016, *A&A*, **594**, A13
- R Core Team 2021, R: A Language and Environment for Statistical Computing. R Foundation for Statistical Computing, Vienna, Austria, <https://www.R-project.org/>
- Riebe K., et al., 2013, *Astronomische Nachrichten*, **334**, 691
- Rines K., Diaferio A., 2006, *AJ*, **132**, 1275
- Rost A., Stasyszyn F., Pereyra L., Martínez H. J., 2020, *MNRAS*, **493**, 1936
- Ruiz A. N., et al., 2015, *ApJ*, **801**, 139
- Salerno J. M., Martínez H. J., Muriel H., 2019, *MNRAS*, **484**, 2
- Salerno J. M., et al., 2020, *MNRAS*, **493**, 4950
- Schaefer A. L., et al., 2017, *MNRAS*, **464**, 121
- Schaye J., et al., 2015, *MNRAS*, **446**, 521
- Schutte Z., Reines A. E., Greene J. E., 2019, *ApJ*, **887**, 245
- Silverman J. D., et al., 2008, *ApJ*, **675**, 1025
- Smith R., et al., 2015, *MNRAS*, **454**, 2502
- Springel V., 2005, *MNRAS*, **364**, 1105
- Springel V., White S. D. M., Tormen G., Kauffmann G., 2001, *MNRAS*, **328**, 726
- Springel V., et al., 2018, *MNRAS*, **475**, 676
- Steinhauser D., Schindler S., Springel V., 2016, *A&A*, **591**, A51
- Stringer M. J., Bower R. G., Cole S., Frenk C. S., Theuns T., 2012, *MNRAS*, **423**, 1596
- Thomas D., Maraston C., Bender R., Mendes de Oliveira C., 2005, *ApJ*, **621**, 673
- Toomre A., 1977, in Tinsley B. M., Larson Richard B. Gehret D. C., eds, *Evolution of Galaxies and Stellar Populations*. p. 401
- Vega-Martínez C. A., Gómez F. A., Cora S. A., Hough T., 2022, *MNRAS*, **509**, 701
- Vijayaraghavan R., Ricker P. M., 2015, *MNRAS*, **449**, 2312
- Villalobos Á., De Lucia G., Murante G., 2014, *MNRAS*, **444**, 313
- Weinmann S. M., van den Bosch F. C., Yang X., Mo H. J., 2006, *MNRAS*, **366**, 2
- Welikala N., Connolly A. J., Hopkins A. M., Scranton R., Conti A., 2008, *ApJ*, **677**, 970
- Wetzel A. R., Tinker J. L., Conroy C., 2012, *MNRAS*, **424**, 232
- Wetzel A. R., Tinker J. L., Conroy C., van den Bosch F. C., 2013, *MNRAS*, **432**, 336
- Whitmore B. C., Gilmore D. M., Jones C., 1993, *ApJ*, **407**, 489
- Wright R. J., Lagos C. d. P., Power C., Stevens A. R. H., Cortese L., Poulton R. J. J., 2022, *MNRAS*, **516**, 2891
- Zheng Z., et al., 2017, *MNRAS*, **465**, 4572
- Zonca A., Singer L., Lenz D., Reinecke M., Rosset C., Hivon E., Gorski K., 2019, *Journal of Open Source Software*, **4**, 1298
- Zwicky F., 1951, *PASP*, **63**, 17
- de los Rios M., Martínez H. J., Coenda V., Muriel H., Ruiz A. N., Vega-Martínez C. A., Cora S. A., 2021, *MNRAS*, **500**, 1784

This paper has been typeset from a $\text{\TeX}/\text{\LaTeX}$ file prepared by the author.